

HIGH ENERGY HEAVY ION COLLISIONS: THE PHYSICS OF SUPER-DENSE MATTER

BARBARA V. JACAK

Department of Physics and Astronomy, SUNY Stony Brook, Stony Brook, NY, 11794, USA

E-mail: jacak@nuclear.physics.sunysb.edu

I review experimental results from ultrarelativistic heavy ion collisions. Signals of new physics and observables reflecting the underlying collision dynamics are presented, and the evidence for new physics discussed. Measurements of higher energy collisions at RHIC are described, and I give some of the very first results.

1 Introduction

High energy heavy ion collisions aim to recreate the conditions which existed a few microseconds following the big bang, and determine the properties of this super-dense matter. The density of produced hadrons is very high; at energy densities of 2-3 GeV/fm³, the inter-hadron distance is smaller than the size of the hadrons themselves. Interactions among hadrons under such conditions are unlikely to be the same as in the familiar dilute hadron gas. QCD predicts that at sufficiently high energy density and temperature, the vacuum “melts” into numerous $q\bar{q}$ pairs.

Such matter is expected to leave the realm where quarks and gluons are confined in colorless hadrons, and form, instead, a quark-gluon plasma. The experiments explore two fundamental puzzles of QCD, namely the confinement of quarks and gluons into hadrons, and the breaking of chiral symmetry which produces mass of the constituent quarks. We aim to study experimentally the nature of deconfined matter, investigate the confinement phase transition, and determine its temperature. The chiral transition is expected to occur under similar conditions. Use of the heaviest ions maximizes the volume and lifetime of matter at high energy density, enhancing signals of new physics. Understanding the background from high energy hadronic collisions, as well as the underlying dynamics and nuclear structure is

accomplished via p+p and p+nucleus collisions in the same detectors.

Solutions of QCD on the lattice have been used to estimate the energy density required for deconfinement.¹ In calculations with three massless quark flavors, a rapid change in the energy density occurs at a critical temperature of 170 ± 10 MeV. The energy density at which the system is fully in the new phase is approximately 3 GeV/fm³. With 2 massless and one strange quark, the critical energy density is 15% lower. Studies have shown that the mass of the $\langle q\bar{q} \rangle$ condensate falls to zero, signifying restoration of chiral symmetry, at about the same temperature.

1.1 Early stage and evolution of the collision

Experimental access to information about the high energy density phase is complicated by the subsequent expansion, cooling and re-hadronization of the matter. Theoretically, however, one may consider several separate stages of a heavy ion collision. Interpenetration and initial nucleon-nucleon collisions are complete in less than 1 fm/c. This is accompanied by multiple parton collisions leading, probably, to local thermal equilibration. The hot, dense matter expands longitudinally and transversely, cooling until the quarks re-hadronize. The hadrons continue to interact among themselves until the system is suffi-

ciently dilute that their mean free path exceeds the size of the collision zone. At this point, hadronic interactions cease and the system “freezes out”.

Elementary nucleon-nucleon collisions have long been studied, and a wealth of data on $p-p$ and $\bar{p}-p$ collisions are in the literature. Quantitative understanding of the initial parton production in heavy ion collisions requires starting with the nucleon quark and gluon structure functions, which are now rather well known from deep inelastic e-p and from p-nucleus experiments.² A steep rise of F_2 , the quark structure function, was discovered² toward low x for $Q^2 \geq 2 \text{ GeV}^2$. This rise is understood to indicate the dominance of gluons, and implies very large numbers of gluon-gluon interactions when two nuclei collide at high energy. H1 at HERA has unfolded the gluon distribution from their data,³ and finds a steep rise at small x . Following this observation, we may expect significant enhancement of gluon fusion processes, such as charm production, for example, in heavy ion collisions. The x and Q^2 regions of interest at RHIC are $x \geq 0.01$ and $Q^2 \approx 10\text{-}20 \text{ GeV}^2$.

It has been observed, however, that structure functions of quarks in nuclei differ from those of nucleons. There is a depletion of quarks in the small- x region, known as “nuclear shadowing”; this effect is expected in gluon distributions also. Shadowing is usually attributed to parton fusion preceding the hard scattering which probes the parton distribution. As the overcrowding at small x is larger in nuclei than in individual nucleons, saturation should be more evident for heavy nuclei, causing shadowing to strengthen with nucleon number. This is indeed the case, and measurements show a 20% modification in heavy nuclei at $x = 0.03$. For Au nuclei, the shadowing in this x region should be a 30% effect. Shadowing may reduce the gluon momentum requiring corresponding enhancement in the large x region if the momen-

tum fraction of gluons is to be conserved. Such “anti-shadowing” has been predicted by Eskola and co-workers, using a DGLAP evolution.⁴ The total number of charged particles produced in a heavy ion collision is sensitive to the magnitude of shadowing and anti-shadowing effects, and can be used to constrain the evolution calculations.

Even with nuclear shadowing, the density of partons after the initial hard nuclear collision is truly enormous, leading us to expect a large amount of multiple parton scattering. Such multiple scattering is already visible in proton-nucleus collisions as the Cronin effect, which hardens the pion p_T spectra above 1.5 GeV/c. The higher parton density in nucleus-nucleus collisions should drive the system toward thermal equilibrium by thermalizing mini-jets and increasing the multiplicity of soft particles. Indeed, parton cascade descriptions of the collision dynamics predict that equilibration among the partonic degrees of freedom happens within 0.3-1 fm/c in collisions at $\sqrt{s} = 200 \text{ GeV}/A$.⁵

The dense medium should affect fast quarks traversing it, and in fact a medium-induced energy loss of partons is expected. As first predicted by Gyulassy and coworkers,⁶ and Baier, Dokshitzer, Mueller, Peigne and Schiff,⁷ the energy loss of a fast quark increases with the density of the medium, due to an accumulation of the transverse momentum transferred. The energy loss dE/dx may exceed 1 GeV/fm, and BDMPS calculated that it could reach $3/\text{times}(L/10\text{fm}) \text{ GeV}/\text{fm}$ at $T = 250 \text{ MeV}$, where L is the path length through the dense medium. Experimental measurements of this energy loss will thus reflect the density of the medium early in the collision.

The quark gluon plasma expands and cools, whereupon the system hadronizes. The deconfined and mixed phases are expected to last approximately 3 fm/c, after which the system becomes a dense, interacting hadron gas. Expansion continues, and the system

finally becomes sufficiently dilute that the hadrons cease to interact approximately 10 fm/c after the start of the collision.⁵

Of course, these values depend strongly upon the assumptions in the models, and the boundaries between phases are not sharp in either time or space. A major experimental challenge is to determine the timescales, along with the duration of hadron emission following freezeout. The expansion velocity is accessible via interferometry; scaling longitudinal expansion ($\beta \approx 1$) along with radial expansion at approximately half the longitudinal velocity have been observed.⁸

1.2 Predicted signals of quark gluon plasma

A number of key predictions for quark gluon plasma signatures were made prior to experiments at CERN and Brookhaven. Color screening by a quark gluon plasma was predicted to suppress bound $c\bar{c}$ pairs, resulting in decreased J/ψ , ψ' and χ_c production.⁹ Observation of this effect is subject to understanding final state interactions of the charmed mesons with nucleons and co-moving hadrons, which break up the bound state.

Rafelski and Mueller predicted in 1982 that production of strange hadrons should be enhanced by formation of quark gluon plasma.¹⁰ The rate of gluon-gluon collisions rises in a hot gluon gas, thereby increasing the cross section of gluon fusion processes and production of strange and charmed quarks. An important hadronic background to this measurement is associated production of strange particles in the dense hadron gas, primarily via $\pi + N \rightarrow K + \Lambda$. Strangeness exchange also complicates the picture.

Thermal electromagnetic radiation reflects the initial temperature of the system, via quark-antiquark annihilation to virtual photons which decay to lepton pairs, and via quark-gluon Compton scattering. The

rate, proportional to T^4 , should be dominated by the initial temperature, T_{init} ; the shape of the spectrum will reflect this maximum temperature. Measurements are difficult because of the large lepton and photon backgrounds from hadron decays, hadronic bremsstrahlung, D meson decays and Drell-Yan pairs.

Possible observable effects of chiral symmetry restoration include modification of meson masses¹¹ (visible through their leptonic decays) and formation of disoriented chiral condensate domains. Such a condensate should result in modified ratios of charged to neutral pions and enhanced production of soft pions with $p_T \leq 100$ MeV/c.¹²

The predicted large energy loss of quarks traversing a very dense medium would result in “quenching” of jets,^{6,7} which can be observed experimentally via the spectrum of hadrons at high p_T . Since such hadrons are dominantly the leading particles in jet fragmentation, their spectrum reflects the spectrum of quarks exiting the medium. This observable reflects the density of the medium, rather than its confinement properties, but experimental evidence for existence of a superdense medium would be most exciting.

1.3 Experimental observables

The charged particle multiplicities in high energy heavy ion collisions are enormous. At SPS energy of $\sqrt{s} = 18\text{-}20$ GeV/A, there are more than 1000 hadrons produced, while at RHIC the number is closer to 10000.

Experimentally accessible observables fall into two classes. The first characterize the system formed and ascertain that the conditions warrant a search for new physics. These observables are primarily hadronic and reflect the system late in the collision. Detailed analysis of hadrons also yields dynamical information about the collision, allowing one to extrapolate the hadronic final state back to the hottest, densest time when quark-

gluon plasma may have existed.¹³

The second class of observables comprises signals of new physics. Lepton pairs and photons (*i.e.* virtual and real photons) decouple from the system early, and emerge undisturbed by the surrounding hadronic matter. Consequently, their distributions are dominated by the early time in the collision, and the rate reflects the initial temperature. Strangeness production can be detected via K , Λ and other hadrons containing strange quarks; multistrange anti-baryons are particularly promising indicators of strangeness enhancement, as it is difficult to affect their production via hadronic means.¹⁴ In a high temperature plasma with many gluons, the gluon fusion reaction $g + g \rightarrow c\bar{c}$ should be important.^{15,16,5} Measurement of semileptonic, or perhaps even fully reconstructed, decays of charmed mesons would indicate whether charm production reflects enhanced gluon fusion.

2 Results for $\sqrt{s} \leq 20$ GeV/nucleon

2.1 Energy Density

Before searching for evidence of deconfinement, we must determine whether appropriate values of energy density are in fact reached. Estimating the energy density 1 fm/c into the collision from measured quantities requires some assumptions. However, this can be done from measured production of energy transverse to the beam direction, $E_T = \Sigma E \sin \theta$. E_T reflects the randomization of the incoming longitudinal energy of the beam. For collisions undergoing scaling longitudinal expansion, the energy density may be estimated via $\epsilon = dE_T/d\eta \times 1/\text{volume}$. The volume is given by the cross sectional area of the nucleus involved, and a length defined by the formation of particles, τ , generally taken to be 1 fm, though this is likely \sqrt{s} dependent, becoming smaller for high energy collisions.

Selecting as central collisions, the few percent of the total cross section producing the largest multiplicity, one may estimate the relevant nuclear area to be $\approx 90\%$ of the total. Using the E_T value of 450 GeV at this point, as measured in Pb + Pb collisions by the NA49 collaboration¹⁷, and $R = 1.2A^{1/3}(0.9)$, with $V = (\pi R^2)\tau$, the energy density, ϵ , is found to be ≈ 3.2 GeV/fm³. This is sufficiently high compared to the predicted transition point, to encourage searching for signals of new physics.

2.2 Color screening

As charmed quarks are produced in the initial hard collisions, they traverse the dense matter and therefore probe its properties. The screening length is directly related to the temperature and energy density, so $c\bar{c}$ bound states of different radius will be screened under different conditions. The J/ψ , with radius of 0.29 fm and binding energy of approximately 650 MeV should be more stable than the ψ' with binding energy of 60 MeV and nearly twice the radius.

Suppression of J/ψ production has been observed by NA50.¹⁸ In light systems, the suppression is consistent with expectations from initial and final state effects on production and binding of the $c\bar{c}$ pairs. However, in Pb + Pb collisions, the suppression is 25% greater than that expected from conventional processes. The anomalous suppression sets in for semi-peripheral Au + Au collisions, and increases in strength with the volume of the excited system.

The observed suppression has been compared with hadronic models as a function of collision centrality (determined by measurement of transverse energy).¹⁹ The measured J/ψ to Drell-Yan ratio decreases in more central collisions, and by $E_T \approx 100$ GeV has fallen well below models which assume charmonium states are absorbed by interactions with comoving hadrons.¹⁹ Figure 1 shows the

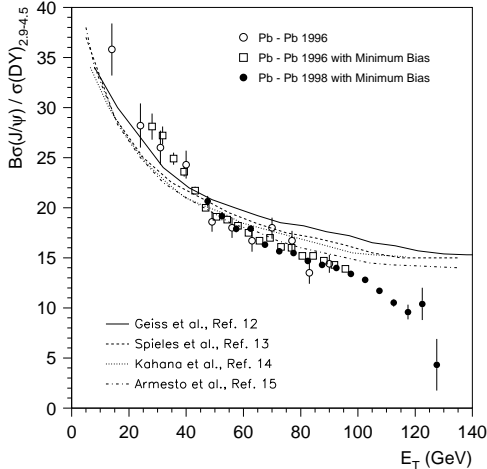


Figure 1. Comparison of NA50 measurement of the ratio of J/ψ and Drell-Yan cross section as a function of E_T (i.e. centrality) in Pb + Pb collisions with several conventional descriptions of J/ψ suppression¹⁹.

measured ratio of J/ψ to Drell-Yan in 158 GeV/A Pb + Pb collisions, as a function of E_T ; high E_T corresponds to central Pb + Pb collisions.¹⁹ The points are data, while the curves show J/ψ production in models which assume that the charmonium states are absorbed by interactions with comoving hadrons.²⁰ Discussion continues within the community regarding discontinuities and thresholds, and a possible second drop of the J/ψ production at $E_T \geq 110$ GeV. Nevertheless, the data very clearly deviate from the hadronic models for central collisions.

2.3 Strangeness enhancement

Strangeness production in a heavy ion collision may not be subject to the well-known strangeness suppression observed in elementary nucleon collisions. This can be easily understood from simple energy level considerations. If the energy levels of u and d quarks are empty, it is energetically favorable to produce these light quarks, since the s quark levels have an energy gap of twice the strange quark mass. In nucleus-nucleus col-

lisions, however, the dense matter causes the lowest u and d quark levels to be filled, resulting in a relative enhancement of strange quark number over p-p collisions.

Enhancement of several species of strange hadrons has been observed. Kaon and Λ enhancement may be expected in a dense hadron gas,²¹ as a result of associated production in hadron multiple scattering, but the excess production of $\bar{\Lambda}$, Ξ and Ω observed by WA97 is not easily explained without new physics.^{22,23} It is particularly remarkable that the enhancement compared to p-nucleus collisions of multiply strange antibaryons increases with the number of strange quarks. In order to achieve such production rates via hadronic equilibration, a dense hadron gas would need to live for about 100 fm/c. Given the measured expansion velocities, such a lifetime is ruled out.

2.4 Thermal radiation

Measurable rates of thermal dileptons and thermal photons were predicted by Shuryak and others.²⁴ The rate is proportional to the fourth power of the temperature, and is thus dominated by the initial (highest) temperature of the system. The distribution of the radiation should have an exponential shape

$$\propto e^{-M/T},$$

and the rate should depend on the square of the particle multiplicity. Consequently, detection of thermal radiation depends strongly on T_{init} achieved in the collisions. Complicating both measurement and interpretation, and boosting the photon emission rate, is partonic bremsstrahlung, which also contributes.²⁵

It is important to note that a hot hadron gas will radiate thermal photons and dileptons as well. Consequently, thermal radiation does not indicate the phase of the matter, but reflects its highest temperature. Experimentally, the goal is to measure the presence of real photons or dileptons, beyond those from

hadronic decays, and from the yield and distributions extract T_{init} . This value is then to be compared to the expected transition temperature.

WA98 observed direct photons beyond contributions from hadronic decays in central Pb + Pb collisions at 158 GeV/nucleon at $p_T \gtrsim 2$ GeV/c.²⁶ A decomposition of the excess photons does not clearly show whether the p_T distribution differs from photons in p-p and p-nucleus collisions, but the enhanced yield appears consistent with $T_{init} > T_C$.^{26,27}

The spectrum of lepton pairs below the ρ meson mass is of considerable interest. Though in p+Be and p+Au collisions the invariant mass distribution of electron-positron pairs below 1 GeV is well described by hadronic decays, a clear excess is observed in S + Au and Pb + Pb collisions by CERES.²⁸ It is difficult to reproduce the observed distribution without allowing the mass of the ρ to change or invoking a tremendous amount of collision broadening, which opens new phase space and effectively lowers the ρ mass.²⁹ Such observations may indicate partial chiral symmetry restoration in the dense matter created in collisions at the SPS.

It may be that the low mass dileptons arise from thermal radiation.³⁰ Excess dileptons in the intermediate mass range between 1 and 3 GeV have also been observed. The intermediate mass lepton pair cross section can be explained if thermal radiation is added to Drell-Yan and charm decay sources.³¹ Both sets of data imply initial temperatures in the range 170-200 MeV. Both calculations make use of parton/hadron duality in the dense system to predict the thermal radiation from simple $q\bar{q}$ annihilation rates, integrating over the time evolution of the collision. Such explanations do not prove that the observed dileptons are thermal in origin, but indicate that the spectra are consistent with an initial temperature near or above the predicted phase transition temperature.

2.5 Evolution of the hadronic phase

The high density of produced particles should create high pressure in the collision, leading to rapid expansion. The expansion velocity can be extracted by combining measurements of single particle m_T distributions with two particle correlations,¹³ requiring a simultaneous fit of both distributions to disentangle flow from thermal motion.

The inverse slopes of single particle spectra are given by

$$T \approx T_{freezeout} + \frac{1}{2}m_0 \langle v_T \rangle^2$$

where $T_{freezeout}$ is the temperature at which the hadronic system decouples (i.e. hadron collisions cease) and $\langle v_T \rangle$ is the average radial expansion velocity.

The two particle correlations measure the size of the region of hadron homogeneity (i.e. full information transport) at freezeout. Position-momentum correlations from expansion case this to be smaller than the entire hadron gas volume. Large statistics are needed for 3-dimensional analysis of the correlation functions, binned in m_T of the particles. The results of such analyses follow approximately

$$R_T^2 = \frac{R^2}{1 + \xi \frac{m_T}{T_{freezeout}} \langle v_T \rangle^2}$$

The freezeout temperature is approximately 100 MeV and the average radial expansion velocity 0.5 c. The data indicate that the system expands by a factor of 3 radially while undergoing a scaling expansion longitudinally. Back-extrapolation from the freezeout conditions, combined with the measured transverse energy yields energy densities of 2-3 GeV/fm³.

If the radial expansion velocity, v_T , indicates pressure created in the collision, v_T should increase with the number of produced particles. Burward-Hoy³² performed a global study of v_T with system size by analyzing single particle spectra below $m_T = 1$ GeV/c; correlation functions are only available for

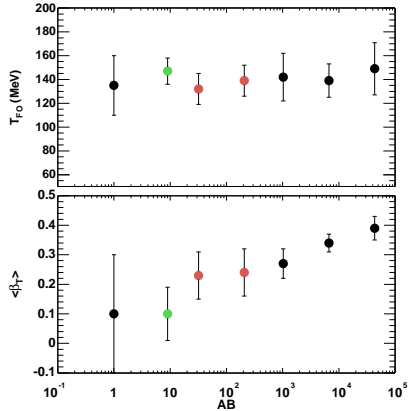


Figure 2. Dependence of freezeout temperature and expansion velocity extracted from π , K, and p spectra below $m_T = 1$ GeV on colliding system size ³².

a small subset of projectile-target combinations. The radial expansion velocity indeed increases with system size, as can be seen in Figure 2, which shows the extracted freezeout temperature and v_T as a function of the number of possible nucleon-nucleon collisions ($A_{projectile} \times A_{target}$). The apparent freezeout temperature is 140 MeV, approximately independent of system size. Radial expansion in the large colliding systems boosts the particles, thus soft physics processes reach larger p_T than in elementary collisions. Consequently, observations of hard scattering will require higher p_T . Burward-Hoy extrapolated the soft spectrum using the T_{FO} and v_T parameters and found that for Pb + Pb at CERN, hard scattering is only a partial contribution to the spectrum below $p_T \approx 5$ GeV/c.³²

2.6 Quark energy loss

Figure 3 shows predictions by X.N. Wang of the effect of quark energy loss on the single particle p_T spectrum.³³ At sufficiently high p_T , where the spectrum is dominated by leading particles from jet fragmentation, energy loss or jet quenching will decrease the yield

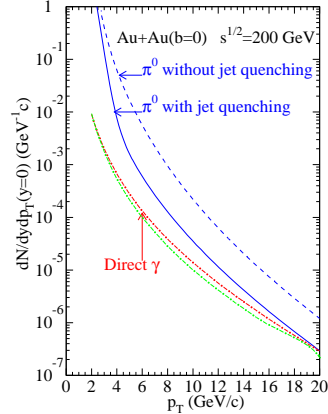


Figure 3. p_T distribution for π^0 with and without parton energy loss as compared to direct photons in central Au + Au at $\sqrt{s} = 200$ GeV/nucleon. $dE/dx = 1$ GeV/fm was used ³³.

of particles by lowering the energy of the fragmenting jet. Comparing the solid and dashed π^0 curves indicates that the difference could be easily measurable already at $p_T = 4$ GeV/c. The lower pair of curves illustrates the small difference expected in the direct photon p_T distribution, indicating that another effect of jet quenching will be to increase γ/π^0 .

At CERN, WA98 measured the π^0 spectrum to nearly 4 GeV/c and did not observe any evidence of jet quenching.³⁴ However, as discussed above, the soft physics likely still contributes significantly at this p_T , masking energy loss effects. As the cross section for hard processes will be considerably larger at RHIC, the spectra should be measurable to considerably higher p_T . Jet quenching will thus be a very important observable at RHIC.

3 Prospects for RHIC

The Relativistic Heavy Ion Collider (RHIC) at Brookhaven National Laboratory began operation in summer 2000. RHIC collided Au beams at $\sqrt{s} = 130$ GeV per nucleon, which will be increased to 200 GeV per nucleon in the next run. RHIC will also collide

smaller nuclei, protons on nuclei, and two polarized proton beams at \sqrt{s} up to 500 GeV. The design luminosity is $2 \times 10^{26}/\text{cm}^2/\text{sec}$ for Au + Au, $10^{31}/\text{cm}^2/\text{sec}$ for p + p and $10^{29}/\text{cm}^2/\text{sec}$ for p + A. Luminosity achieved during the first run reached 10% of design value.

Higher energy and long running time at RHIC will allow in-depth investigation of the currently tantalizing observables. With the factor ten increase in center of mass energy, every collision should be well above the phase transition threshold. The initial temperature can be expected to significantly exceed estimates of T_C . Furthermore, hard processes which provide probes of the early medium have considerably higher cross sections. Consequently, experiments will be able to measure J/ψ and other hard processes to higher p_T with better statistical significance than before. Charged and neutral pion spectra at $p_T \geq 5\text{GeV}$ to look for evidence of jet quenching will be accessible, and the γ/π^0 ratio will reach the p_T range where direct photon yields are calculable.

3.1 Experiments at RHIC

To cover the full range of experimental observables, RHIC has a suite of four experiments. There are two large and two small experiments, each optimized differently. Together, they form a comprehensive program to fully characterize the heavy ion collisions and search for all the predicted signatures of deconfinement and chiral symmetry restoration.

Each experiment is outfitted with two zero-degree calorimeters of identical design. These calorimeters measure neutral particles produced at zero degrees, allowing a common method of selecting events according to centrality. An event sample with interesting behavior observed by one experiment can therefore be checked by the other experiments. Many of the hadronic observables are mea-

sured by two or more of the experiments, so a complete picture of the collisions at RHIC will be investigated.

The two small experiments, PHOBOS and BRAHMS, focus on difficult-to-measure regions of rapidity and p_T . PHOBOS is optimized to measure and identify hadrons at very low p_T and fits on a (large) table top. The low p_T capability provides good sensitivity to formation of disoriented chiral condensates. In addition, PHOBOS has a full coverage multiplicity measurement, allowing analysis of fluctuations and selection of events with unusually numerous particles. Particle tracking is done primarily with highly granular silicon detectors, allowing very short flight paths and minimizing decay of the low p_T hadrons. Identification is accomplished by time-of-flight measurements.

BRAHMS maps particle production over a wide range of rapidities with good p_T coverage. BRAHMS has two movable, small acceptance spectrometers to sample the particle distributions; a typical event has only a few particles in each spectrometer. Tracking is provided by modest size time projection chambers and drift chambers. Particle identification is performed via time-of-flight measured by scintillator hodoscopes and via gas Cherenkov threshold counters.

The two large experiments each measure many of the predicted QGP signatures, along with observables to map the hadronic phase. STAR has maximum acceptance for hadrons, allowing event-by-event analyses of the final state and reconstruction of multi-strange hadron decays. PHENIX is optimized for photon and lepton detection and has high rate capability and selective triggers to collect statistics on rare processes.

STAR consists of a large acceptance time projection chamber, covering full azimuth over two units of rapidity centered around mid-rapidity (90 degrees in the laboratory). The TPC sits in a solenoidal magnetic field. In the second and third years of RHIC run-

ning, a silicon vertex tracker and electromagnetic calorimeters will be added to improve the efficiency of finding secondary vertices and to allow measurement of jets. In the first year, STAR had a partial acceptance ring-imaging Cherenkov counter to identify a subset of the particles and trigger on high p_T hadrons. STAR events include dense information on each of many charged particle tracks and are consequently very large; approximately one event per second is written.

PHENIX has multiple subsystems to track, identify, and trigger on leptons, photons, and hadrons. At midrapidity, there is an axial field magnet with two detector sectors, each covering 90 degrees in azimuth. Drift, pad, and time expansion chambers provide tracking, scintillator hodoscope time-of-flight detectors for hadron identification, a large ring-imaging Cherenkov counter identifies electrons, and a highly granular electromagnetic calorimeter is used for electron and photon identification and triggers. Charged particle multiplicity and fluctuations are measured with silicon detectors. Forward and backward, PHENIX has two cone-shaped magnets outfitted with cathode strip detectors for tracking and Iarocci tubes interleaved with steel plates for muon identification. The pole tips of the central magnet absorb approximately 90% of the hadrons. PHENIX began running with the central arms and silicon detectors, with muon measurements commencing in 2001.

3.2 First Results

Figure 4 shows a central Au + Au collision at $\sqrt{s} = 130$ GeV/nucleon, recorded in the STAR TPC.³⁵ The large number of tracks illustrates the challenges for the experiments. All experiments reconstruct tracks with good efficiency. STAR has demonstrated successful particle identification via dE/dx in these collisions. PHENIX, with excellent granularity ($\Delta\eta = \Delta\phi = 0.01$) and resolu-

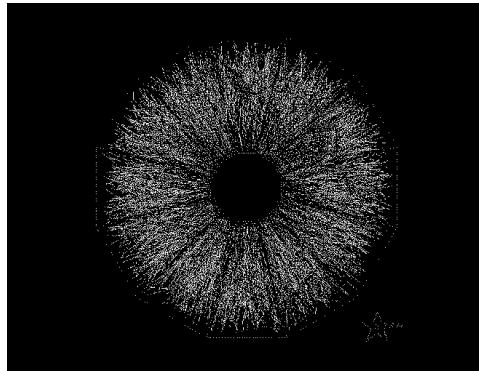


Figure 4. Display of a central Au + Au collision at $\sqrt{s} = 130$ GeV/nucleon in the STAR time projection chamber³⁵.

tion ($\approx 8\%/\sqrt{E}$) calorimetry, reconstructs π^0 and transverse energy distributions from such events with high particle multiplicity.

The PHOBOS Collaboration has measured the charged particle rapidity density at midrapidity for the 6% most central Au + Au collisions. They find $dN/d\eta = 555 \pm 12(\text{stat.}) \pm 35(\text{syst.})$ at $\sqrt{s} = 130$ GeV/nucleon.³⁶ The importance of this first measurement can be appreciated by looking at the variation in predicted particle multiplicity for $\sqrt{s} = 200$ GeV/nucleon in the literature³⁷ and for $\sqrt{s} = 130$ GeV/nucleon in Figure 5.³⁷ The range of predictions is almost a factor of 2! Three important factors control the total number of charged particles produced at midrapidity: parton multiple scattering (which increases the multiplicity), nuclear shadowing (the effect is very sensitive to the x and Q^2 dependence), and energy loss in the dense medium (energy loss tends to increase the number of soft particles at the expense of p_T in the tail of the distribution).

The PHOBOS result shows excellent agreement with the HIJING model of Wang using quark energy loss $dE/dx = 1$ GeV/fm, gluon $dE/dx = 0.5$ GeV/fm and nuclear shadowing taken from lower \sqrt{s} measurements.³³ The anti-shadowing prescription of Eskola and coworkers clearly

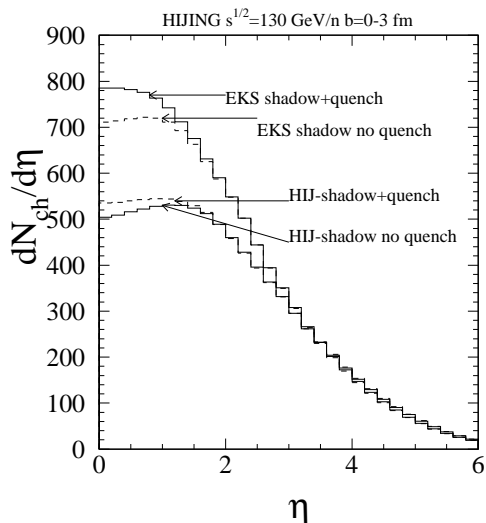


Figure 5. Charged particle multiplicity distribution predicted by HIJING for central Au + Au collisions at $\sqrt{s} = 130$ GeV/nucleon. Different curves correspond to different assumptions of nuclear shadowing and parton energy loss ³⁷.

overpredicts the multiplicity. Of course, it is difficult to crisply separate three components with a single data point. The p_T spectrum of hadrons will constrain the parton energy loss in these collisions; analyses are currently underway. The shadowing can be determined directly by measurement of hadron yields at $p_T = 2 - 6$ GeV/c in proton-nucleus and proton-proton collisions.³⁸ However, at this point we may tentatively conclude that (unless Nature has conspired to provide some exact cancellations) that nuclear shadowing appears to saturate and no anti-shadowing occurs.

4 Conclusions

I have shown that experiments produce dense interacting matter in the laboratory and that we can extract physics from the very complex interactions between heavy ions. One may ask whether the quark gluon plasma has been observed in collisions near $\sqrt{s} = 20$ at CERN, and the answer must needs be “prob-

ably”. Several predicted signatures have been independently measured which defy currently available conventional explanations. Correlated onset has not been demonstrated, however. The lack of a coherent theoretical description and the incompleteness of appropriate dynamic theories make unambiguous conclusions difficult. Still missing is experimental determination of the energy threshold for deconfinement, and characterization of the properties of the quark gluon plasma state.

The experimental program in the coming years has its work clearly cut out: We must determine T_{init} from electromagnetic radiation, measure the jet quenching and learn to untangle the soft from the hard physics. Observation of multiple signatures at the same condition will be crucial, and a measurement of the hadron formation transition would be most helpful. RHIC has begun operation, and will contribute greatly via an experimental program with common event selection to constrain theory via a suite of observables.

Acknowledgments

I would like to thank Axel Drees, Xin-Nian Wang, Thomas Ullrich and Sam Aronson for valuable discussions and figures for the talk. This work was supported by the U.S. Department of Energy under grant number DE-FG02-96ER40988.

References

1. F. Karsch, E. Laermann and A. Peikert, *Phys. Lett. B* **478**, 447 (2000).
2. M. Klein in *Proceedings of Lepton-Photon Symposium*, Stanford, Calif. August 1999, and references therein.
3. C. Adloff, et al. (H1 Collaboration), *Nucl. Phys. B* **545**, 21 (1999).
4. K.J. Eskola, V.J. Kolhinen and P.V. Ruuskanen, *Nucl. Phys. B* **535**, 351 (1998); K.J. Eskola, V.J. Kolhinen and C.A. Sal-

- gado, *Eur. Phys. J. C* **9**, 61 (1999).
5. K. Geiger, *Phys. Rev. D* **48**, 4129 (1993).
 6. M. Gyulassy and M. Pluemer, *Phys. Lett. B* **243**, 432 (1990); X.N. Wang and M. Gyulassy, *Phys. Rev. Lett.* **68**, 1480 (1992).
 7. R. Baier, Yu.L. Dokshitzer, A.H. Mueller, S. Peigne and D. Schiff, *Nucl. Phys. B* **483**, 291 (1997); *Nucl. Phys. B* **484**, 265 (1997).
 8. H. Appelshäuer, et al. (NA49 Collaboration), *Eur. Phys. J C* **2**, 661 (1998).
 9. T. Matsui and H. Satz, *Phys. Lett. B* **178**, 416 (1986).
 10. J. Rafelski and B. Mueller, *Phys. Rev. Lett.* **48**, 1066 (1982).
 11. G.E. Brown and Mannque Rho, *Phys. Lett. B* **237**, 3 (1990).
 12. K. Rajagopal and F. Wilczek, *Nucl. Phys. B* **399**, 395 (1993); *Nucl. Phys. B* **404**, 577 (1993).
 13. U. Heinz and B.V. Jacak, *Ann. Rev. of Nucl. Part. Sci.* **49**, 529 (1999).
 14. H.C. Eggers and J. Rafelski, *Int. J. Mod. Phys. A* **6**, 1067 (1991).
 15. B. Mueller and X.N. Wang, *Phys. Rev. Lett.* **68**, 2437 (1992).
 16. B. Kaempfer, et al., *J. Phys. G* **23**, 2001 (1997).
 17. H. Appelshäuser, et al., *Phys. Rev. Lett.* **75**, 3814 (1995).
 18. M.C. Abreu, et al. (NA50 Collaboration), *Phys. Lett. B* **410**, 327 and 337 (1997).
 19. M.C. Abreu, et al. (NA50 Collaboration), *Phys. Lett. B* **477**, 28 (2000).
 20. J. Geiss, et al. *Phys. Lett. B* **447**, 31 (1999); C. Spieles, et al., *Phys. Rev. C* **60**, 054901 (1999); D. E. Kahana and S. H. Kahana, *Prog. Part. Nucl. Phys.* **42**, 269 (1999) and nucl-th/9908063; N. Armesto, A. Capella and E. G. Ferreira, *Phys. Rev. C* **59**, 395 (1999).
 21. H. Sorge, et al., *Phys. Lett. B* **271**, 37 (1991).
 22. S. Abatzis, et al. (WA85 Collaboration), *Phys. Lett. B* **270**, 123 (1992).
 23. E. Andersen, et al. (WA97 Collaboration), *Phys. Lett. B* **433**, 209 (1998).
 24. E. Shuryak, *Phys. Lett. B* **78**, 150 (1978).
 25. P. Aurenche, D. Gelis, H. Zavaket and R. Kobes, *Phys. Rev. D* **58**, 085003 (1998).
 26. M. M. Aggarwal, et al. (WA98 Collaboration), nucl-ex/0006008 and nucl-ex/0006007, (2000).
 27. D. Srivastava and B. Sinha, nucl-th/0006008 (2000).
 28. G. Agakichiev et al. (CERES Collaboration), *Phys. Rev. Lett.* **75**, 1272 (1995); *Phys. Lett. B* **422**, 405 (1998).
 29. G.E. Brown, G.Q. Li, R. Rapp, M. Rho and J. Wambach, *Acta Phys. Polon. B* **29**, 2309 (1998).
 30. B. Kaempfer, K. Gallmeister and O.P. Pavlenko, hep-ph/0001242.
 31. R. Rapp and E. Shuryak, *Phys. Lett. B* **473**, 13 (2000).
 32. J. Burward-Hoy and B. Jacak, to be published.
 33. X.N. Wang, *Phys. Rev. C* **58**, 2321 (1998).
 34. M.M. Aggarwal, et al. (WA98 Collaboration), *Phys. Rev. Lett.* **81**, 4087 (1998).
 35. <http://www.star.bnl.gov>, and T. Ullrich, private communication.
 36. B. Back, et al. (PHOBOS Collaboration), *Phys. Rev. Lett.* **85**, 3100 (2000).
 37. X.N. Wang, *Nucl. Phys. A* **661**, 210c (1999); X.N. Wang and Miklos Gyulassy, nucl-th/0008014 (2000); X.N. Wang, private communication.
 38. X.N. Wang, *Phys. Rev. C* **61**, 064910 (2000).